Title
Preferential Stripping of a Lithium Protrusion Resulting in Recovery of a Planar Electrode

Journal
Journal of The Electrochemical Society, 167(10)

ISSN
0013-4651

Authors
Maslyn, Jacqueline A
McEntush, Kyle D
Harry, Katherine J
et al.

Publication Date
2020-01-06

DOI
10.1149/1945-7111/ab9d62

Peer reviewed

Preferential Stripping of a Lithium Protrusion Resulting in Recovery of a Planar Electrode

Jacqueline A. Maslyn [1, 2, *], Kyle D. McEntush [1], Katherine J. Harry [3], Louise Frenck [1, *], Whitney S. Loo [1], Dilworth Y. Parkinson [4], Nitash P. Balsara [1, 2, 5, z, *]

[1] Department of Chemical and Biomolecular Engineering, University of California, Berkeley, California 94720, USA

[2] Materials Sciences Division, Lawrence Berkeley National Laboratory, Berkeley, California, 94720, USA

[3] Department of Materials Science and Engineering, University of California, Berkeley, California 94720, USA

[4] Advanced Light Source, Lawrence Berkeley National Laboratory, Berkeley, California 94720, USA

[5] Energy Technologies Area, Lawrence Berkeley National Laboratory, Berkeley, California 94720, USA

[z] Corresponding author. [nbalsara@berkeley.edu]

*ECS member

Abstract Text

Lithium metal is a high-energy-density battery electrode material, but the largely irreversible growth of lithium protrusions on an initially planar electrode during cycling makes it unsuitable for incorporation into a commercial battery. In this study, a lithium electrode with globular protrusions was stripped electrochemically, and the local morphology of the electrode as a function of time was determined by hard X-ray tomography. We demonstrate that globules are preferentially stripped compared to a planar electrode in our system, which incorporates a nanostructured block copolymer electrolyte. We report current density at the electrode as a function of micron-scale position and time. The local current density during the electrode healing process calculated from a reference frame at the electrode/electrolyte interface provides insight into the driving forces responsible for selective stripping of the globule. These results imply the possibility of discharging protocols that may return a lithium electrode to its initial planar state.

Introduction

Rechargeable batteries with lithium metal anodes are of interest for their higher energy densities compared to conventional lithium-ion batteries.[1–4] Two primary differences between electrodes in conventional lithium-ion and lithium metal anodes are, first, the non-negligible displacement of the electrode/electrolyte interface as the anode is charged and discharged, and second, the spontaneous formation of protrusions at the electrode during charging, the so-called "dendrite problem". During cycling, these electronically conductive protrusions increase in size, reducing cell efficiency and possibly causing short-circuit cell failure.[5,6]

Lithium electrodeposition from liquid electrolytes leads to the formation of filamentous,

dendritic structures and mossy lithium, depending on factors such as current density, pressure, electrolyte spacer, temperature, electrolyte composition.[7–10] The theoretical work of Monroe and Newman first established the idea that the formation of lithium protrusions may be suppressed by sufficiently rigid electrolytes: suppression is predicted to occur when the forces that cause non-planar deposition are overwhelmed by the mechanical force exerted by the deformed solid electrolyte.[11–17] Since lithium is a relatively soft metal, finding electrolytes with nominal moduli that satisfy this condition is not difficult. For example, at room temperature, the ceramic electrolyte $Li_7La_3Zr_2O_{12}$ (LLZO) has a shear modulus of about 60 GPa, which is a factor of 14-18 higher than that of lithium metal.[12,18,19] In spite of this, lithium protrusions push through this material, particularly through grain boundaries.[20–22] Lithium protrusions also occur in rigid block copolymer electrolytes, but they have a globular shape due to mechanical suppression of the protrusion by the electrolyte.[23–26] The growth of lithium protrusions has been a topic of theoretical interest in all three types of electrolytes (liquid, polymeric, ceramic).[27–33]

At sufficiently high current densities, the formation of non-planar deposits during lithium plating appears inevitable. One question we seek to answer is whether or not one might heal a lithium electrode where nonplanar deposition has occurred. It seems intuitively obvious that anodes with branched, filamentous structures cannot be returned to a planar state; experimental results support this thought.[7–9] Simpler geometries like globules may, in principle, be "healed" and returned to a planar morphology. Much of the literature on lithium metal anodes is focused on solving the dendrite problem arising during plating, although lithium stripping is an important factor in cell behavior.[34] This study is differentiated as follows: first, we visualize and quantify the healing of lithium metal anodes during stripping; second, we also

view protrusions from a moving reference frame attached to the electrode/electrolyte interface.

Experimental

The polystyrene-*block*-poly(ethylene oxide) (PS-PEO, or SEO) diblock copolymer was synthesized and characterized as described previously.[35–37] The number averaged molecular weights of the PS and PEO blocks were 200 and 222 kg mol^{-1}, respectively. The neat PEO volume fraction of the SEO copolymer is 0.51. The overall polydispersity index of the polymer is 1.08 measured by gel permeation chromatography (GPC) using PS standards in N-Methyl-2-pyrrolidone (NMP).

Methods for electrolyte preparation and electrochemical cell fabrication are identical to those previously described.[25,26] The molar ratio of lithium salt, lithium bis(trifluoromethanesulfonyl)imide (LiTFSI), to ethylene oxide in the electrolyte is 0.085. All electrolyte preparation and cell assembly was carried out in argon gloveboxes (MBraun) with less than 0.1 parts per million (ppm) H_2O and less than 0.1 ppm O_2.

We present data on a lithium/SEO-LiTFSI/lithium symmetric cell. All cycling and polarization experiments were conducted at 90 °C. The symmetric cell was subjected to 14 conditioning cycles at 0.02 mA cm^{-2} before the polarization and tomography experiment.[25,26] The thickness of lithium transferred between the electrodes in each half cycle during conditioning was 0.4 μm. The cell was polarized in one direction at a constant current of 0.175 mA cm^{-2} to nucleate and grow globular protrusions. The polarization was suspended before cell failure by short-circuit, and the direction of polarization was reversed in order to strip lithium from the nucleated globules. Details of the polarization routine used for the cell is reported in Table 1. At multiple points during this process, the cells were imaged using X-ray tomography

at beamline 8.3.2 of the Advanced Light Source at Lawrence Berkeley National Laboratory: cells were visualized after conditioning cycles, after initial polarization, and several times during the reverse polarization. Details of imaging and reconstruction have been reported previously.[23,25,26,38] Cells were cycled away from the beamline and imaged in separate experiments that were conducted in approximately 1-month intervals due to limited availability of beamtime. While we took care to physically realign the cell as closely as we could over the course of these experiments, some differences were inevitable. The X-ray beam and optics are also not identical for each experiment.

For quantitative analysis, reconstructed features of interest at different time points were digitally aligned in space using the commercially available Avizo software package using at least three independent features of reference. The aligned volumes containing the features of reference were cropped such that the volume was constant in size and position over time. These volumes were labeled and imported into MATLAB for analysis. Electrolyte thickness was calculated by subtracting the z (vertical) position of the upper and lower electrode/electrolyte interfaces at a single time point. Thickness of deposited lithium was calculated by subtracting the z (vertical) positions of an electrode/electrolyte interface at two different time points. The current density at a pixel at position (j,k) in the xy plane, i_{jk}, was calculated using the volume of lithium deposited at that pixel, V_{jk}:

$$i_{jk} = \frac{V_{jk}\rho F}{M_{Li}at} \quad (1)$$

where ρ is the density of lithium metal, F is the Faraday constant, M_{Li} is the molecular weight of lithium metal, a is the pixel area, and t is time. This analysis builds on that previously reported by Harry et al.[14]

Results and Discussion

Direct imaging during electrochemical cycling is necessary to understand how protrusions evolve over time.[9,23,39–46] Here, lithium/polymer electrolyte/lithium symmetric cells were imaged using time-resolved hard X-ray tomography. The solid polymer electrolyte used in this study was a polystyrene-*block*-poly(ethylene oxide) (PS-PEO, or SEO) copolymer mixed with lithium bis(trifluoromethanesulfonyl)imide (LiTFSI): see experimental methods for details. The images thus obtained are shown in Figure 1. The cell was initially polarized for 155 h so that lithium was electrodeposited on the bottom electrode and a globule developed. Then, at $t = 0$, the cell was reverse polarized such that lithium is stripped from the bottom electrode and plated on the top electrode. Details of the polarization routine are given in Table 1. Figure 1a presents 3-D renderings of the volume of interest as a function of the duration of lithium stripping. Figures 1b and 1c show slices through the cell in the *xz* and *yz* planes, respectively. The bright polymer electrolyte is a horizontal stripe between two dark layers of lithium metal. A bright sac composed of reacted electrolyte material distinguishes the lithium globule from the rest of the electrode. As stripping proceeds, the portion of the globule protruding above the lower electrode/electrolyte interface decreases until the surface of the globule becomes level with the rest of the electrode. Figure 1d maps the interelectrode distance (or electrolyte thickness), L, in the *xy* plane over time. Yellow stripes represent grain boundaries in the lithium metal, where no electrochemical deposition took place. At $t = 0$, the globule is initially represented by the thin spot in the electrolyte in dark blue. Over time, as the globule is preferentially stripped, the electrolyte recovers and L becomes more uniform. The average interelectrode distance, L_{avg}, was computed at each time point using the data in Fig. 1d. It is

evident that L away from the globule is constant (within experimental error) during the stripping process.

Figure 2 maps experimentally determined local current density in the *xy* plane; the method is discussed in the experimental section. The roughly circular cross-section of the globule at the lower electrode/electrolyte interface at $t = 0$ is marked with a white outline and is reproduced on all plots. Our approach for determining current density leads to artifacts at lithium grain boundaries; to a good approximation, grain boundaries are not electrochemically active. These artefacts can be seen as three lines that appear to project radially outward from the globule. The time stamps associated with each panel in Fig. 2 correspond to the midpoint time in the interval over which the current density was determined. At $t = 5$ h and $t = 16$ h, it is evident that the local current density is slightly higher at the globule than the surrounding planar electrode. Hot spots at the edge of the globule are apparent as orange lines. At $t = 27$ h, the hot spot is focused at the center of the globule tip, implying a rapid decrease in the protrusion height and a return of the electrode to a nearly planar geometry. This is corroborated by the $t = 32$ h images in Fig. 1, which represent the end of the $t = 27$ h time-step. At $t = 37$ h, the current density is much more uniform and the planar geometry of the stripped electrode is maintained. For each time-step, the average calculated current densities at the top and bottom electrodes are equal within 2-18% percent. However, when comparing time-steps, the current density varies both above and below the average current density as recorded by the potentiostat, 0.175 mA cm^{-2}. The reason for the local variations in current density are not clear. It may be related to stresses exerted on the electrode or plastic deformation of the polymer. It is worth

noting that a 1-pixel error in segmentation over a 10-hour time-step would lead to a 0.03 mA cm^{-2} miscalculation in current density.

Figure 3a. shows a view of the globule during stripping from a frame of reference outside the cell, including the location of the lower electrode/electrolyte interface at $t = 0$ and $t = 42$ h. From this frame of reference, the interface moves downward in the z direction as lithium is removed from the bottom electrode and plated on the top electrode. The inset shows a magnified view of the globule with the electrolyte surfaces removed. The distances between globule interfaces represent the total amount of lithium stripped from the globule between time-points. The black arrows indicate signatures of areas around the globule perimeter with higher current densities than the surrounding area obtained at $t = 5$ and $t = 16$ h – the "hot spots" identified in Fig. 2 as yellow-orange streaks near the edge of the globule. This results in notches in the globule at $t = 10$ and $t = 22$ h.

Fig. 3b shows a view of the globule surface during stripping from the frame of reference of the lower electrode/electrolyte interface. Here, the differences in lithium volume between time-points represent the excess lithium stripped from the globule (beyond the amount of lithium stripped from the planar electrode). The corresponding local current directly quantifies how the electrode heals. The globule interface at $t = 42$ h is level with the surrounding electrode/electrolyte interface.

The average current density over the globule, i_{glob}, was calculated by averaging the current in the region plotted and outlined in white in Fig. 2. The average current density over the planar electrode, i_{plane}, was calculated in the same way with respect to the region exterior

to the globule. The total area within which these current densities are calculated is 325 x 325 μm^2 (the same area plotted in Fig. 1d). In Fig. 4a, we plot i_{glob} and i_{plane} as a function of time. Both i_{glob} and i_{plane} increase from *t = 0* to *t = 27* h, during which the majority of electrode healing occurs. Next, we plot in Fig. 4b the excess current density, defined as $i_{\mathrm{excess}} = i_{\mathrm{glob}} - i_{\mathrm{plane}}$, which quantifies lithium flux as observed from the reference frame attached to the electrode/electrolyte interface. i_{excess} is approximately constant around 0.028 mA cm^{-2} between *t = 0* to *t = 27* h, and then drops to half that value at *t = 37* h. The drop in i_{excess} signals the end of the healing process as a function of time. Fig. 4c reports the normalized excess current, $i_{\mathrm{n}} = \frac{i_{\mathrm{excess}}}{i_{\mathrm{plane}}}$, as a function of time of lithium stripping. This parameter decreases continuously during the healing process. At early times, the distance between the tip of the globule and the upper electrode is at a minimum and the strain in the polymer is at a maximum: both factors would enhance i_{n}. The observed decrease in i_{n} as healing continues reflects the reduction in both the driving forces that are responsible for healing.

Conclusions

A lithium electrode with globular protrusions was stripped electrochemically and the time-dependence of the local morphology of the electrode was determined by hard X-ray tomography. In our system, which incorporates a nanostructured block copolymer electrolyte, we demonstrate that recovery of a planar lithium electrode occurs naturally. We calculate the local current density as a function of time and position in the vicinity of the globule. An excess current density observed from a reference frame attached to the electrode/electrolyte interface quantifies the flattening of the globule. We demonstrate that a suitably normalized excess

current density decreases as the protrusion shrinks due to a decrease in the driving forces for healing. Our conclusions are based on a detailed analysis of one globule. It is desirable to quantify the dynamics of stripping of a large ensemble of globules. We hope accomplish this in future studies. In spite of the limitations of our work thus far, it demonstrates that it may be possible to develop discharging protocols with the purpose of returning a lithium electrode to its initial planar state.

Acknowledgments

This work was supported by the Assistant Secretary for Energy Efficiency and Renewable Energy, Office of Vehicle Technologies of the U.S. Department of Energy under Contract DE-AC02-05CH11231 under the Advanced Battery Materials Research Program (BMR). Hard X-ray experiments were performed at the Advanced Light Source which is supported by the Director, Office of Science, Office of Basic Energy Sciences, of the U.S. Department of Energy under Contract No. DE-AC02-05CH11231. JAM was supported by a National Science Foundation Graduate Research Fellowship DGE-2752814. LF acknowledges funding from the Energy & Biosciences Institute through the EBI-Shell program. WSL was supported by a National Science Foundation Graduate Research Fellowship DGE-1106400.

References

1. D. Aurbach, E. Zinigrad, H. Teller, and P. Dan, *J. Electrochem. Soc.*, **147**, 1274–1279 (2000)

2. L. Gireaud, S. Grugeon, S. Laruelle, B. Yrieix, and J. M. Tarascon, *Electrochem. commun.*, **8**, 1639–1649 (2006).

3. D. Lin, Y. Liu, and Y. Cui, *Nat. Nanotechnol.*, **12**, 194–206 (2017).

4. N. P. Balsara and J. Newman, *J. Chem. Educ.*, **90**, 446–452 (2013).

5. X.-B. Cheng, R. Zhang, C.-Z. Zhao, and Q. Zhang, *Chem. Rev.*, **117**, 10403–10473 (2017).

6. J. Liu, Z. Bao, Y. Cui, E. J. Dufek, J. B. Goodenough, P. Kalifah, Q. Li, B. Y. Liaw, P. Liu, A. Manthiram, Y. S. Meng, V. R. Subramanian, M. F. Toney, V. V. Viswanathan, M. S. Whittingham, J. Xiao, W. Xu, J. Yang, X. Yang, J. Zhang, *Nat. Energy*, **4**, 180–186 (2019).

7. J. Steiger, D. Kramer, and R. Mönig, *Electrochim. Acta*, **136**, 529–536 (2014).

8. J. Steiger, G. Richter, M. Wenk, D. Kramer, and R. Mönig, *Electrochem. commun.*, **50**, 11–14 (2015).

9. K. N. Wood, E. Kazyak, A. F. Chadwick, K. H. Chen, J. G. Zhang, K. Thornton, N. P. Dasgupta, *ACS Cent. Sci.*, **2**, 790–801 (2016).

10. L. Frenck, G. K. Sethi, J. A. Maslyn, and N. P. Balsara, *Front. Energy Res.*, **7**, 115 (2019).

11. C. Monroe and J. Newman, *J. Electrochem. Soc.*, **150**, A1377–A1384 (2003).

12. C. Monroe and J. Newman, *J. Electrochem. Soc.*, **152**, A396–A404 (2005).

13. G. M. Stone, S. A. Mullin, A. A. Teran, D. T. Hallinan, A. M. Minor, A. Hexemer, N. P. Balsara, *J. Electrochem. Soc.*, **159**, A222–A227 (2012).

14. K. J. Harry, K. Higa, V. Srinivasan, and N. P. Balsara, *J. Electrochem. Soc.*, **163**, 2216–2224 (2016).

15. P. Barai, K. Higa, and V. Srinivasan, *Phys. Chem. Chem. Phys.*, **19**, 20493–20505 (2017)

16. P. Goyal and C. W. Monroe, *J. Electrochem. Soc.*, **164**, E3647–E3660 (2017).

17. M. Ganser, F. E. Hildebrand, M. Klinsmann, M. Hanauer, M. Kamlah, and R. M. McMeeking, *J. Electrochem. Soc.*, **166**, H167-176 (2019).

18. J. E. Ni, E. D. Case, J. S. Sakamoto, E. Rangasamy, and J. B. Wolfenstine, *J. Mater. Sci.*,

47, 7978–7985 (2012).

19. S. Yu, R. D. Schmidt, R. Garcia-Mendez, E. Herbert, N. J. Dudney, J. B. Wolfenstine, J. Sakamoto, D. J. Seigel, *Chem. Mater.*, **28**, 197–206 (2016).

20. M. Nagao, A. Hayashi, M. Tatsumisago, T. Kanetsuku, T. Tsuda, and S. Kuwabata, *Phys. Chem. Chem. Phys.*, **15**, 18600–18606 (2013).

21. L. Porz, T. Swamy, B. W. Sheldon, D. Rettenwander. T. Frömling, H. L. Thaman, S. Berendts, R. Uecker, W. C. Carter, Y. M. Chiang, *Adv. Energy Mater.*, **7**, 1–12 (2017).

22. E. J. Cheng, A. Sharafi, and J. Sakamoto, *Electrochim. Acta*, **223**, 85–91 (2017).

23. K. J. Harry, D. T. Hallinan, D. Y. Parkinson, A. A. Macdowell, and N. P. Balsara, *Nat. Mater.*, **13**, 69–73 (2013)

24. K. J. Harry, X. Liao, D. Y. Parkinson, A. M. Minor, and N. P. Balsara, *J. Electrochem. Soc.*, **162**, A2699–A2706 (2015)

25. J. A. Maslyn, W. S. Loo, K. D. McEntush, H. J. Oh, K. J. Harry, D. Y. Parkinson, N. P. Balsara, *J. Phys. Chem. C*, **122**, 26797–26804 (2018)

26. J. A. Maslyn, L. Frenck, W. S. Loo, D. Y. Parkinson, and N. P. Balsara, *ACS Appl. Energy Mater.*, **2**, 8197–8206 (2019).

27. R. Akolkar, *J. Power Sources*, **232**, 23–28 (2013)

28. A. Aryanfar, D. Brooks, B. V. Merinov, W. A. Goddard, A. J. Colussi, and M. R. Hoffmann, *J. Phys. Chem. Lett.*, **5**, 1721–1726 (2014).

29. Y. Takeda, O. Yamamoto, and N. Imanishi, *Electrochemistry*, **4**, 210–218 (2016).

30. A. Jana and R. E. García, *Nano Energy*, **41**, 552–565 (2017)

31. F. Hao, A. Verma, and P. P. Mukherjee, *ACS Appl. Mater. Interfaces*, **10**, 26320–26327

(2018).

32. A. Jana, S. I. Woo, K. S. N. Vikrant, and R. E. Garcı, *Energy Environ. Sci.*, **12**, 3595–3607 (2019).

33. L. Barroso-Luque, Q. Tu, and G. Ceder, *J. Electrochem. Soc.*, **167**, 020534 (2020).

34. M. J. Wang, R. Choudhury, and J. Sakamoto, *Joule*, **3**, 2165–2178 (2019)

35. R. P. Quirk, J. Kim, C. Kausch, and M. Chun, *Polym. Int.*, **39**, 3–10 (1996).

36. N. Hadjichristidis, H. Iatrou, S. Pispas, and M. Pitsikalis, *J. Polym. Sci. Part A Polym. Chem.*, **38**, 3211–3234 (2000).

37. M. Singh, O. Odusanya, G. M. Wilmes, H. B. Eitouni, E. D. Gomez, A. J. Patel, V. L. Chen, M. J. Park, P. Fragouli, H. Iatrou, N. Hadjichristidis, D. Cookson, N. P. Balsara, *Macromolecules*, **40**, 4578–4585 (2007)

38. R. J. Pandolfi, D. B. Allan, E. Arenholz, L. Barroso-Luque, S. I. Campbell, T. A. Caswell, A. Blair, F. De Carlo, S. Fackler, A. P. Fournier, G. Freychet, M. Fukuto, D. Gursoy, Z. Jiang, H. Krishnan, D. Kumar, R. J. Kline, R. Li, C. Liman, S. Marchesini, F. Ren, S. Sahoo, J. Strzalka, D. Sunday, C. J. Tassone, D. Ushizima, S. Venkatakrishnan, K. G. Yager, P. Zwart, J. A. Sethian, A. Hexemer, *J. Appl. Synchrotron Radiat.*, **25**, 1261–1270 (2018).

39. C. Brissot, M. Rosso, J.-N. Chazalviel, P. Baudry, and S. Lascaud, *Electrochim. Acta*, **43**, 1569–1574 (1998)

40. C. Brissot, M. Rosso, J.-N. Chazalviel, and S. Lascaud, *J. Electrochem. Soc.*, **146**, 4393–4400 (1999)

41. D. S. Eastwood, P. M. Bayley, H. J. Chang, O. O. Taiwo, J. Vila-Comamala, D. J. L. Brett, C. Rau, P. J. Withers, P. R. Shearing, *Chem. Commun.*, **51**, 266–268 (2015).

42. O. O. Taiwo, D. P. Finegan, J. M. Paz-Garcia, D. S. Eastwood, A. G. Bodey, C. Rau, S. A. Hall, D. J. L. Brett, P. D. Lee, P. R. Shearing, *Phys. Chem. Chem. Phys.*, **19**, 22111–22120 (2017).

43. F. Sun, L. Zielke, H. Markötter, A. Hilger, D. Zhou, R. Moroni, R. Zengerle, S. Thiele, J. Banhart, I. Manke, *ACS Nano*, **10**, 7990–7997 (2016).

44. P. Pietsch and V. Wood, *Annu. Rev. Mater. Res.*, **47**, 451–481 (2017).

45. J. Tippens, J. Miers, A. Afshar, J. A. Lewis, F. Javier, Q. Cortes, H. Qiao, T. S. Marchese, C. V. Di Leo, C. Saldana, M. T. McDowell, *ACS Energy Lett.*, **4**, 1475–1483 (2019).

46. Y. Song, J. Hu, J. Tang, W. Gu, L. He, and X. Ji, *ACS Appl. Mater. Interfaces*, **8**, 32031–32040 (2016).

Tables

Table 1. Method used to obtain time-resolved lithium stripping information. Imaging occurred at each of the time-points provided in the table. Polarization and reverse polarization steps were both conducted at 0.175 mA cm^{-2}.

Time of polarization	Charge passed		Calculated height of lithium
[h]	*[C cm^{-2}]*	*[mA h cm^{-2}]*	*[µm]*
155	97.6	27.1	131.6
Time of reverse polarization	Charge passed		Calculated height of lithium
[h]	*[C cm^{-2}]*	*[mA h cm^{-2}]*	*[µm]*
0	0	0	0
10	6.30	1.75	8.49
22	13.9	3.85	18.7
32	20.2	5.60	27.2

42	26.5	7.35	35.6

1

2

Figures

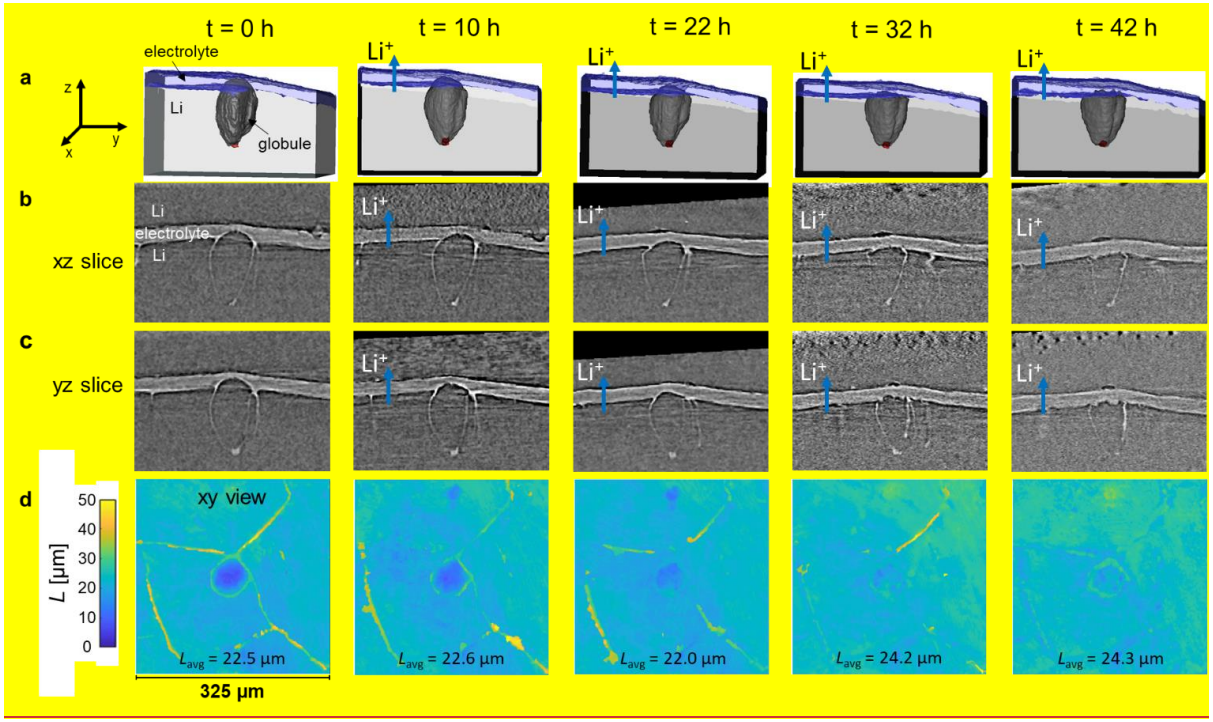

Figure 1. Preferential stripping of a lithium globule after 0, 10, 22, 32, and 42 hours of reversed polarization. (a) 3-D volume renderings of lithium being stripped from an electrode and globule over time. The polymer electrolyte is rendered in purple, the lower lithium electrode in light gray, the globule in dark gray. The upper electrode is transparent. (b) Slices in the xz plane showing lithium being stripped from the bottom electrode and plated on the upper electrode. (c) Slices of the same in the yz plane. (d) Maps of interelectrode distance, *L*, in the *xy* plane. The thin spot in dark blue corresponds to the globule, while the thick lines in yellow correspond to grain boundaries in the lithium.

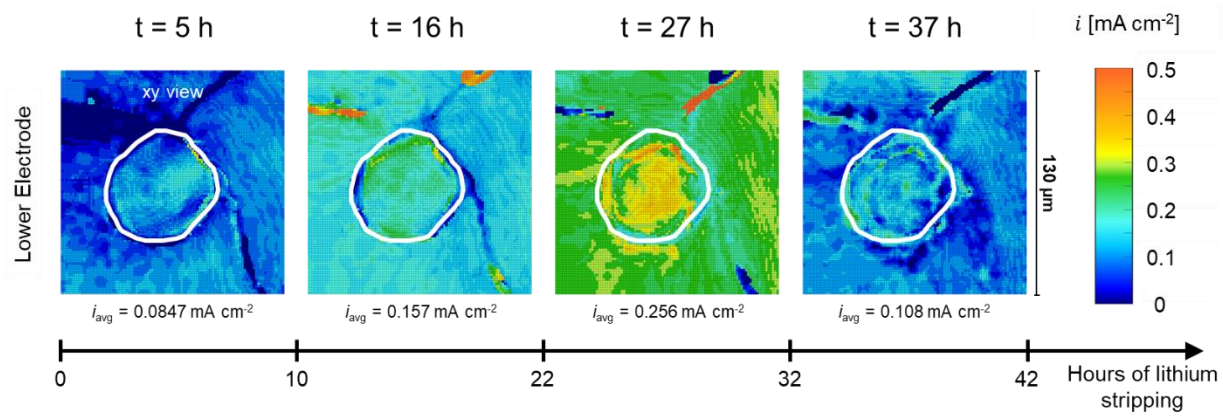

Figure 2. Experimentally calculated current density, i, as a function of position in the *xy* plane and time, enabled by comparing tomograms reported in Fig. 1 as marked in the timeline at the bottom of the figure. The superimposed white outline indicates the location of the globule at $t = 0$. The average current density, i_{avg}, for the area and time step of interest is reported below the plot.

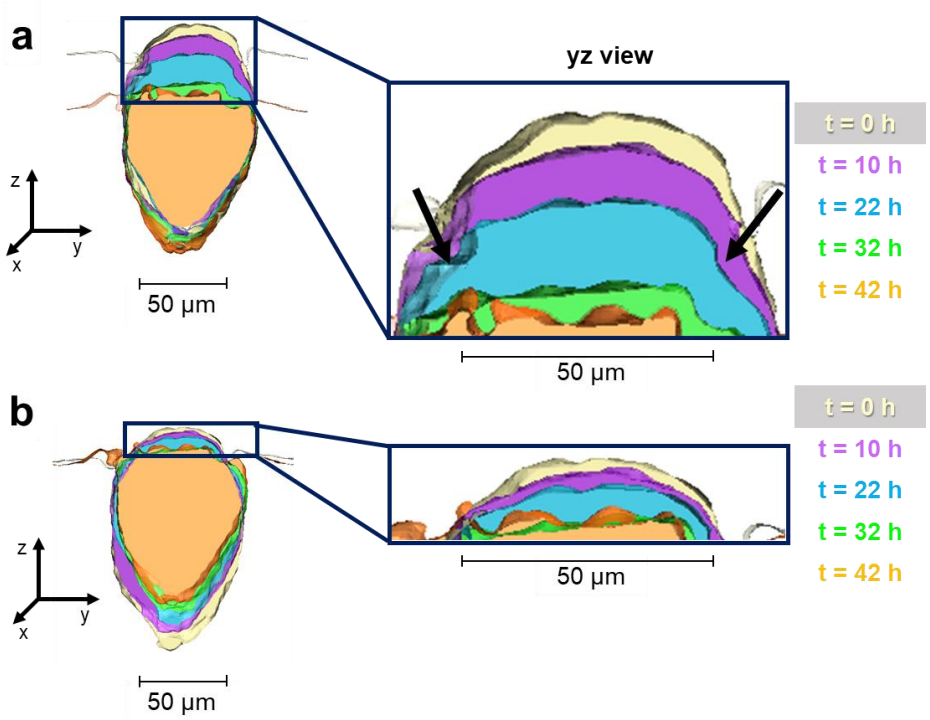

Figure 3. Stripping of the lithium globule as a function of time. The surface of the globule after 0, 10, 22, 32, and 42 hours of stripping is rendered in white, fuchsia, blue, green, and orange, respectively. (a) From a frame of reference outside the cell, the globule shrinks as the electrode/electrolyte interface is translated downward in the z direction. The electrode/electrolyte interfaces at $t = 0$ and $t = 42$ h are shown in white and orange, respectively. The inset provides further detail, and black arrows indicate "hot-spots" with a higher local current density. (b) From the frame of reference of the lower electrode/electrolyte interface, the portion of the globule protruding into the electrolyte becomes smaller over time.

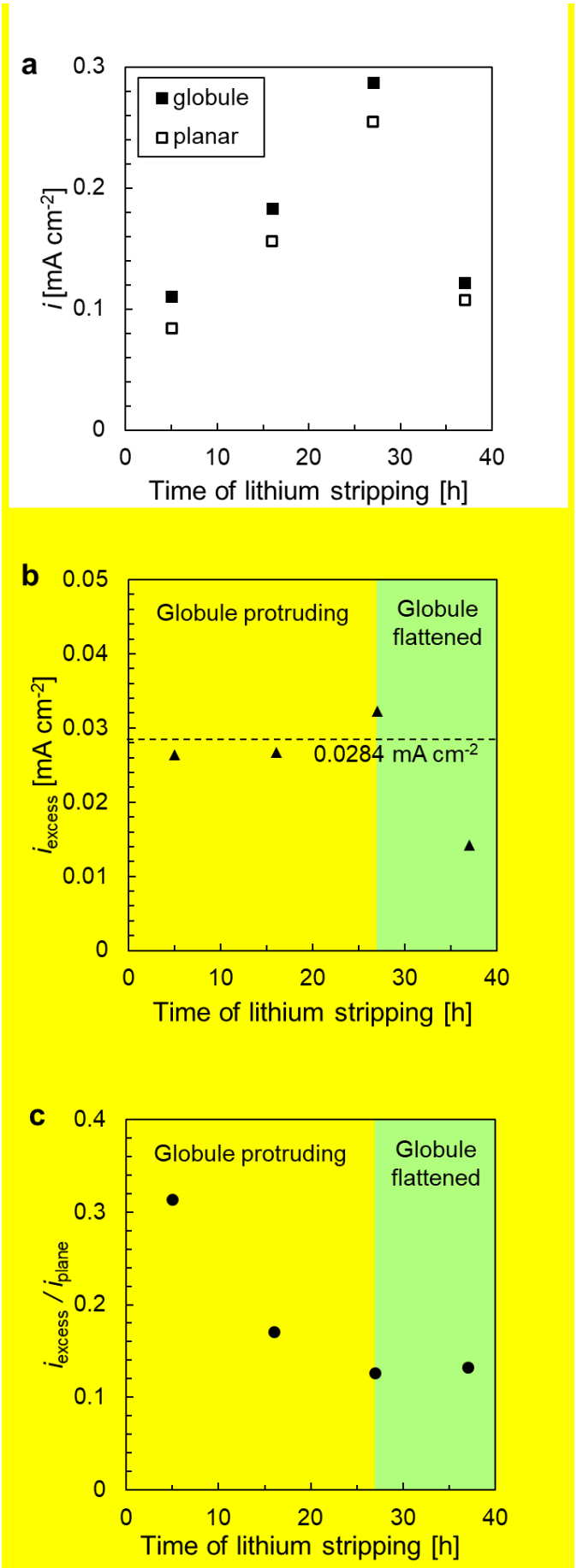
a
0.3
0.2
0.1
0
globule
planar
i [mA cm-2]
0
10
20
30
40
Time of lithium stripping [h]
b
0.05
0.04
0.03
0.02
0.01
0
Globule protruding
Globule flattened
0.0284 mA cm-2
iexcess [mA cm-2]
0
10
20
30
40
Time of lithium stripping [h]
c
0.4
0.3
0.2
0.1
0
Globule protruding
Globule flattened
iexcess / iplane
0
10
20
30
40
Time of lithium stripping [h]

1

Figure 4. Quantification of current density at the globule and surrounding planar electrode. (a) The current density averaged over the area of the globule (filled-in square) and the non-globule area (hollow square) is plotted as a function of time of lithium stripping. (b) Plot of $i_{\text{excess}} = i_{\text{glob}} - i_{\text{plane}}$ with the y-axis rescaled. The dashed line indicates 0.0284 mA cm^{-2}, the average value of between $t = 0$ and $t = 32$ h. By $t = 27$ h of stripping, the lithium electrode is roughly planar. (c) Plot of normalized excess current, $i_{\text{n}} = \frac{i_{\text{excess}}}{i_{\text{plane}}}$, as a function of time of lithium stripping.